

A Sandwich Model for Changing-Look AGNs

QIAN-QI MA,¹ WEI-MIN GU,¹ ZHEN-YI CAI,^{2,3} XINWU CAO,⁴ JUN-XIAN WANG,^{2,3} ZHI-XIANG ZHANG,¹ AND
MOUYUAN SUN¹

¹*Department of Astronomy, Xiamen University, Xiamen, Fujian 361005, People's Republic of China; guwm@xmu.edu.cn*

²*CAS Key Laboratory for Research in Galaxies and Cosmology, Department of Astronomy, University of Science and Technology of China, Hefei 230026, People's Republic of China*

³*School of Astronomy and Space Science, University of Science and Technology of China, Hefei 230026, People's Republic of China*

⁴*Institute for Astronomy, School of Physics, Zhejiang University, 866 Yuhangtang Road, Hangzhou 310058, People's Republic of China*

ABSTRACT

The spectral variability of changing-look active galactic nuclei (CL-AGNs) occurred on timescales of years to tens of years, posing a significant challenge to the standard thin disk model. In this work, we propose a sandwich model, including an optically thick disk in the mid-plane (Disk 1) and two disks of low effective optical depth on both sides (Disk 2). These two types of disks are coupled with magnetic fields, which allow viscous torque interaction between them. As a consequence, the radial velocity of Disk 1 can increase by up to three orders of magnitude compared to the standard thin disk, leading to an equivalent decrease in the accretion timescale. Therefore, such a sandwich model can account for the rapid variability in CL-AGNs. In addition, we also discuss the influence of the magnetic pressure on Disk 2. When Disk 2 is dominated by the magnetic pressure, it resembles a “warm corona”, which is responsible for the soft X-ray excess.

Keywords: Accretion (14) — Active galactic nuclei (16) — Galaxy accretion disks (562) — Black hole physics (159)

1. INTRODUCTION

Active galactic nuclei (AGNs) are the bright cores of galaxies, and their radiation energy comes from the accretion of supermassive black holes (SMBHs). Based on the presence or absence of broad emission lines, AGNs are classified as Type 1 and Type 2 (Seyfert 1943). According to the AGN unification model, differences in the width of emission lines are caused by the different sightline effect (e.g., Urry & Padovani 1995; Osterbrock & Ferland 2006). According to this model, all AGNs should have clear types because the sightline remains unchanged. However, observations in the past few decades have shown that some AGNs experienced Seyfert-type transitions on the timescales of several months to several decades (e.g., Cohen et al. 1986; Denney et al. 2014; MacLeod et al. 2016; Yang et al. 2018; Trakhtenbrot et al. 2019), and some even experienced multiple changes (e.g., McElroy et al. 2016; Oknyansky et al. 2019; Wang et al. 2020). These AGNs are called changing-look AGNs (CL-AGNs). In addition to the variations of the broad emission lines, CL-AGNs often exhibit multi-wavelength variations. These variations were discovered in mid-infrared (e.g., Sheng et al. 2017; Stern et al. 2018; Yang et al. 2019; Wang et al. 2022; Jiang et al. 2021), UV (e.g., Zetzl et al. 2018; Neustadt et al. 2023), and X-ray (e.g., LaMassa et al. 2015; Mathur et al. 2018; Parker et al. 2019; Liu et al. 2022; Liang et al. 2022) bands.

The physical mechanism of CL-AGNs remains a mystery. Several hypotheses have been proposed and some of them successfully explain specific CL-AGNs or a class of them. A straightforward explanation is that the broad line region is obscured by moving clouds or tori in the line of sight of the observer (e.g., Goodrich & Miller 1989; Elitzur 2012), but only a few CL-AGNs can be explained by this scenario (e.g., Ichikawa et al. 2015; Yang et al. 2018; Wang et al. 2019). Another popular scenario is the tidal disruption event (TDE) (Merloni et al. 2015), which has successfully explained some CL-AGNs (e.g., Wyrzykowski et al. 2017; Ricci et al. 2020; Sheng et al. 2021; Zhang 2022). However, TDE is not applicable to some repetitive CL-AGNs and the quasi-periodic outbursts (e.g., Kim et al. 2018; Parker et al. 2019; Hutsemékers et al. 2020; Li et al. 2022). In addition, close binaries of supermassive black holes (CB-SMBHs) with high eccentricities may trigger CL events (e.g., Kim et al. 2018; Wang & Bon 2020), but this scenario is only capable of

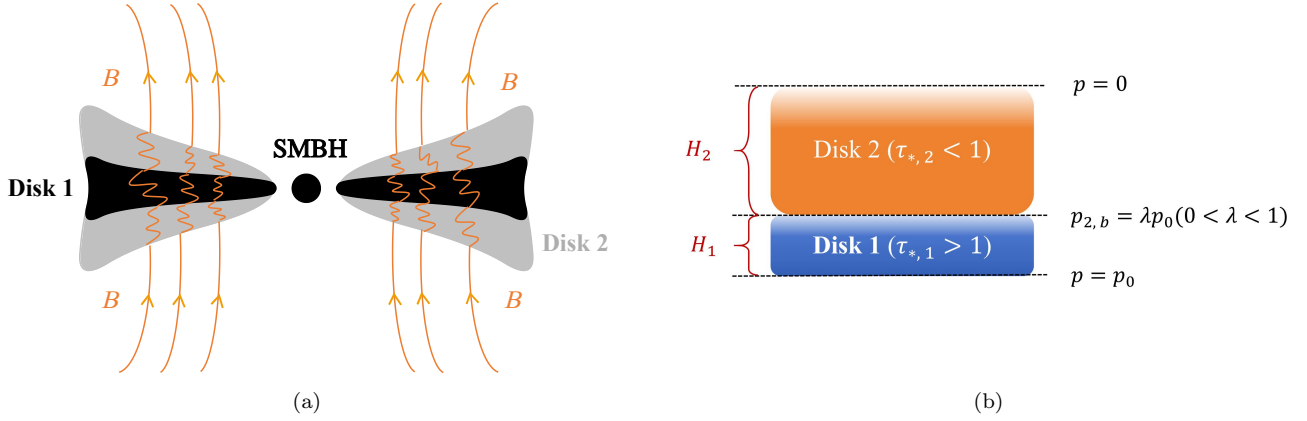


Figure 1. An illustration of the sandwich model. We propose that the Disk 1 and Disk 2 are coupled in the z direction via magnetic fields, as shown in (a), while (b) annotates several key parameters in the z direction.

the periodic CL events. Kim et al. (2018) proposed that Mrk 1018 is an oscillating recoiled SMBH which has a highly eccentric orbit with a period of 29 years, and Wang & Bon (2020) suggested that some CL-AGNs are close binary systems and the CL timescales are related to the orbital periods. On the other hand, the dramatic random fluctuation of the extreme ultraviolet emission is another plausible explanation for CL-AGNs (e.g., Cai et al. 2018, 2020; Sun et al. 2020).

In addition, the rapid changing of the accretion can also create CL events, which is consistent with their multi-wavelength variations and polarization invariance (e.g., MacLeod et al. 2016; Parker et al. 2016; Husemann et al. 2016; Zetzl et al. 2018; Noda & Done 2018; Hutsemékers et al. 2019; Liu et al. 2022; Jin et al. 2022). However, the accretion timescale for the standard thin disk (SSD; Shakura & Sunyaev 1973) is longer than 10^3 yr in the UV/optical area, which is inconsistent with the observed CL timescale. Some other accretion models were proposed to explain the short timescales of CL events, which can be divided into stable and unstable models. For the former scenario, Dexter & Begelman (2019) proposed that magnetically elevated disk has shorter inflow timescale. Following this hypothesis, Feng et al. (2021), Wu & Gu (2023) and Cao et al. (2023) suggested that the magnetic disk-outflows can effectively carry away the angular momentum and decrease the accretion timescale. For the latter scenario, Sniegowska et al. (2020) put forward an ADAF (advection-dominated accretion flow)-SSD model which has a narrow unstable radial zone between ADAF and SSD. They argued that the repeating outbursts in some CL-AGNs are related to the radiation instability in the unstable zone. Based on this model, Pan et al. (2021) proposed that large-scale magnetic fields can significantly shorten the period of outbursts, explaining the quasi-periodic eruptions.

In this work, we construct a sandwich model, including an optically thick disk (Disk 1), with two optically thin disks (Disk 2) above it on both sides, as shown in Figure 1. The “optically thin” and “optically thick” mentioned here refer to the effective optical depth, defined as $\tau_* = \sqrt{\tau_{\text{es}}\tau_{\text{ff}}}$, where τ_{es} and τ_{ff} are electron scattering and free-free absorption optical depth, respectively. Disk 2 has higher radial velocity, which drags Disk 1 through magnetic coupling and increases the radial velocity of Disk 1. This mechanism can decrease the accretion timescale of Disk 1 by three to four orders of magnitude. In addition, we also discuss the impact of the magnetic pressure in Disk 2. When the magnetic pressure is negligible in Disk 2, its temperature will reach to 10^9 K, which resembles a “hot corona” (e.g., Haardt & Maraschi 1993; Liu et al. 2002). However, when the magnetic pressure is more than 10 times greater than the gas pressure, Disk 2 manifests itself a “warm corona”, which may explain the soft X-ray excess phenomenon in AGNs (e.g., Róźańska et al. 2015; Kubota & Done 2018; Ghosh et al. 2022; Ballantyne et al. 2024). We describe our model and the basic equations in Section 2. The numerical results and figures are presented in Section 3. Our conclusions and discussion are presented in Section 4.

2. MODEL

We describe the model in the cylindrical coordinate system (r, ϕ, z) , and the equations of Disk 1 and Disk 2 are presented in the following subsections. The symbols with subscript “1” and “2” respectively represent Disk 1 and Disk 2, and the subscript “0” represents the equatorial plane. The input and output parameters are listed in Tables 1 and 2, respectively.

Table 1. Input parameters

Parameter	Value	Meaning
α	0.1	viscosity parameter
β_{m}	$0 \sim 100$	the ratio of magnetic pressure in Disk 2
η	0.1	energy conversion efficiency
κ_{es}	$0.4 \text{ cm}^2 \text{ g}^{-1}$	electron scattering opacity
r	$50 r_{\text{s}}$	radius
M	$10^7, 10^8 M_{\odot}$	mass for SMBH
\dot{M}	$0.01 \sim 0.1 \dot{M}_{\text{Edd}}$	accretion rate (total)
\dot{M}_2/\dot{M}	$0.01 \sim 0.5$	accretion rate proportion of Disk 2
v_1/v_2	$10^{-3} \sim 1$	radial velocity ratio

NOTE—The input parameters in our model. The symbols, values and meaning of the parameters are listed in the first, second, and third column, respectively.

Table 2. Output parameters

Parameter	Meaning
Ω_{K}	angular velocity
λ	the ratio of the pressures
I	interaction stress
$t_{\text{acc},1}$	accretion timescale of Disk 1
v_1, v_2	radial velocity
$p_0, p_{2,\text{b}}$	pressure
$\rho_0, \rho_{2,\text{b}}$	density
$T_0, T_{2,\text{b}}$	temperature
H_1, H_2	half thickness
Σ_1, Σ_2	surface density
Π_1, Π_2	pressure integration
$T_{r\phi,1}, T_{r\phi,2}$	vertically integrated stress
$\tau_{\text{es},1}, \tau_{\text{es},2}$	electron scattering optical depth
$\tau_{\text{ff},1}, \tau_{\text{ff},2}$	free-free absorption optical depth
$\tau_{*,1}, \tau_{*,2}$	effective optical depth

NOTE—The Output parameters in our model. The symbols and meanings of the parameters are listed in the first and second column, respectively.

2.1. *Optically Thick Disk (Disk 1)*

The equations of Disk 1 are based on the SSD model, and this disk can be described as a “radially faster SSD”. We assume this disk maintains Keplerian rotation and the angular velocity is

$$\Omega_{\text{K}} = \sqrt{\frac{GM}{r^3}}, \quad (1)$$

where M is the central object mass, r is the cylindrical radius, and G is the gravitational constant. The disk maintains hydrostatic equilibrium in the vertical direction, therefore the gravity and the pressure are balanced with each other, and the hydrostatic equilibrium equation is

$$\frac{dp}{dz} = -\frac{GM}{r^3}\rho z, \quad (2)$$

where p and ρ are the pressure and the density, with z , the vertical coordinate (Hōshi 1977). To describe the changing of p and ρ in the z direction, we employ the polytropic relation $p = K\rho^{1+1/N}$ (K and N are constants) in the vertical direction (Hōshi 1977; Kato et al. 2008), and we assume $N = 2$ (Narayan & Yi 1995; Narayan et al. 1997). Using $p = \lambda p_0$ ($0 < \lambda < 1$) at $z = H_1$ (H_1 is the half thickness of Disk 1) as the boundary conditions, we can get the solutions of p and ρ from Equation (2) for Disk 1, respectively expressed as $p_1(z)$ and $\rho_1(z)$:

$$p_1(z) = p_0 \cdot [1 - (1 - \lambda^{\frac{1}{N+1}})\frac{z^2}{H_1^2}]^{N+1} \quad (0 < z < H_1), \quad (3)$$

$$\rho_1(z) = \rho_0 \cdot [1 - (1 - \lambda^{\frac{1}{N+1}})\frac{z^2}{H_1^2}]^N \quad (0 < z < H_1), \quad (4)$$

where p_0 and ρ_0 are the pressure and density at $z = 0$, respectively. By integrating Equations (3) and (4), we can get the pressure integration, $\Pi_1 = 2 \int_0^{H_1} p_1(z) dz$, and the surface density, $\Sigma_1 = 2 \int_0^{H_1} \rho_1(z) dz$.

The pressures in Disk 1 at $z = 0$ include gas and radiation pressures, expressed as

$$p_0 = \frac{\rho_0 k_B T_0}{\mu m_H} + \frac{1}{3} a T_0^4, \quad (5)$$

where T_0 is the temperature at $z = 0$ (Kato et al. 2008), μ , m_H , k_B and a respectively represent the mean molecular weight ($\mu = 0.5$), the hydrogen atom mass, the Boltzmann constant, and the radiation constant. From Equations (2), (3) and (4), we can get the equation for H_1 ,

$$\Omega_K^2 H_1^2 = 2(N+1)(1 - \lambda^{\frac{1}{N+1}})\frac{p_0}{\rho_0}, \quad (6)$$

where $2(N+1)(1 - \lambda^{\frac{1}{N+1}})$ is the integration constant.

The continuity equation is

$$\dot{M}_1 = -2\pi r v_1 \Sigma_1, \quad (7)$$

where \dot{M}_1 is the accretion rate of Disk 1, and v_1 is the radial velocity of Disk 1 (Kato et al. 2008, Chapter 3.2). The angular momentum equation is

$$\dot{M}_1(r^2 \Omega_K - j) = -2\pi r^2 T_{r\phi,1}, \quad (8)$$

where j is the specific angular momentum per unit mass swallowed by the black hole, and $T_{r\phi,1} = -(\alpha \Pi_1 + I)$ is the vertically integrated stress exerted on Disk 1, where I is the interaction between the two disks caused by the magnetic fields in the $r\phi$ -plane, and α is the viscosity parameter.

The thermal equilibrium of Disk 1 is expressed as

$$Q_{\text{vis},1}^+ = Q_{\text{rad},1}^-, \quad (9)$$

where $Q_{\text{vis},1}^+$ is the viscous heating rate per unit area, and $Q_{\text{rad},1}^-$ is the radiation cooling rate per unit area, respectively. They are expressed as

$$Q_{\text{vis},1}^+ = r T_{r\phi,1} \frac{d\Omega_K}{dr}, \quad (10)$$

$$Q_{\text{rad},1}^- = \frac{8acT_0^4}{3\tau_1}, \quad (11)$$

where $\tau_1 = \int_0^{H_1} \kappa_1 \rho_1(z) dz$, and $\kappa_1 = \kappa_{\text{es},1} + \kappa_{\text{ff},1}$ is the opacity of Disk 1. We employ $\kappa_{\text{es},1} = 0.4 \text{ cm}^2 \text{ g}^{-1}$ and $\kappa_{\text{ff},1} = 6.4 \times 10^{22} \bar{\rho}_1 \bar{T}_1^{-3.5} \text{ cm}^2 \text{ g}^{-1}$ as the electron scattering and free-free absorption opacities respectively, where $\bar{\rho}_1$ and \bar{T}_1 are the average quantities in the z direction (Kato et al. 2008, Chapter 7.2). Disk 1 is dominated by the electron scattering opacity, thus $\kappa_1 \sim \kappa_{\text{es},1}$.

2.2. *Optically Thin Disk (Disk 2)*

We employ an optically thin accretion flow for Disk 2. This disk is geometrically thick, cooled by radiation and advection. The accretion rate of Disk 2 is lower than Disk 1, and thus the proportion of Disk 2 is $\dot{M}_2/\dot{M} \leq 0.5$, where $\dot{M} = \dot{M}_1 + \dot{M}_2$ is the total accretion rate and \dot{M}_2 is the accretion rate of Disk 2.

Equations (1) and (2) are also employed for the angular velocity and the hydrostatic equilibrium in z direction, respectively. Integrating Equation (2) from $z = H_1$ to $z = H_1 + H_2$, with the same polytropic relation as Disk 1, and $p = 0$ at $z = H_1 + H_2$ as the boundary conditions, we can get the solutions of p and ρ for Disk 2, respectively expressed as $p_2(z)$ and $\rho_2(z)$:

$$p_2(z) = p_{2,b} \cdot \left[1 - \frac{z^2 - H_1^2}{(H_1 + H_2)^2 - H_1^2}\right]^{N+1} \quad (H_1 < z < H_1 + H_2), \quad (12)$$

$$\rho_2(z) = \rho_{2,b} \cdot \left[1 - \frac{z^2 - H_1^2}{(H_1 + H_2)^2 - H_1^2}\right]^N \quad (H_1 < z < H_1 + H_2), \quad (13)$$

where $p_{2,b}$ and $\rho_{2,b}$ are the pressure and density at the bottom of Disk 2, respectively. To ensure the continuity of pressure in z direction, $p_{2,b} = \lambda p_0$. In the z direction, $p_{2,b}$ corresponds to the maximum pressure for Disk 2, and $\rho_{2,b}$ corresponds to the maximum density.

The pressures in Disk 2 include gas and magnetic pressures. Assuming that $\beta_m = p_{\text{mag},2}/p_{\text{gas},2}$, the pressure of Disk 2 is

$$p_{2,b} = p_{\text{gas},2b} + p_{\text{mag},2b} = (1 + \beta_m)p_{\text{gas},2b}, \quad (14)$$

where $p_{\text{gas},2b} = \rho_{2,b} k_B T_{2,b}/\mu m_H$, and we assume that β_m is constant in z direction. According to the simulation results by Jiang et al. (2014), and the theoretical investigation for the magnetic pressure in the warm corona by Róžańska et al. (2015), a corona dominated by magnetic pressure can form above a gas pressure dominated disk, and $p_{\text{mag}}/p_{\text{gas}}$ can exceed to 100 in the corona. Therefore we employ the value for β_m ranging from 0 to 100, while in Disk 1 we assume that the magnetic pressure is negligible. From Equations (2), (12) and (13), we can get the equation for H_2 ,

$$\Omega_K^2 (H_2^2 + 2H_1 H_2) = 2(N+1) \frac{p_{2,b}}{\rho_{2,b}}, \quad (15)$$

where the integration factor is $2(N+1)$. The pressure integration can be estimated as $\Pi_2 = 2 \int_{H_1}^{H_1+H_2} p_2(z) dz$, and the surface density can be estimated as $\Sigma_2 = 2 \int_{H_1}^{H_1+H_2} \rho_2(z) dz$. The continuity equation has the same form as Equation (7), expressed as

$$\dot{M}_2 = -2\pi r v_2 \Sigma_2, \quad (16)$$

where v_2 is the radial velocity for Disk 2. And the angular momentum equation is

$$\dot{M}_2 (r^2 \Omega_K - j) = -2\pi r^2 T_{r\phi,2}, \quad (17)$$

where $T_{r\phi,2} = -(\alpha \Pi_2 - I)$ is the vertically integrated stress exerted on Disk 2.

The thermal equilibrium of Disk 2 is

$$Q_{\text{vis},2}^+ = Q_{\text{adv},2}^- + Q_{\text{rad},2}^-, \quad (18)$$

where $Q_{\text{vis},2}^+$ is the viscous heating rate per unit area, $Q_{\text{adv},2}^-$ is the advection cooling rate and $Q_{\text{rad},2}^-$ is the bremsstrahlung radiation cooling rate, respectively expressed as

$$Q_{\text{vis},2}^+ = r T_{r\phi,2} \frac{d\Omega_K}{dr}, \quad (19)$$

$$Q_{\text{adv},2}^- = \frac{\dot{M}_2}{2\pi r^2} \frac{\Pi_2}{\Sigma_2} \xi, \quad (20)$$

$$Q_{\text{rad},2}^- = Q_{\text{brem}}^- = 0.23 \times (1.24 \times 10^{21} \rho_{2,b}^2 H_2 T_{2,b}^{1/2}) \text{ erg s}^{-1} \text{ cm}^{-2}, \quad (21)$$

where ξ is

$$\xi = -\left[\left(A + \frac{1}{2}\right) \frac{d \ln \Pi_2}{d \ln r} - \left(A + \frac{3}{2}\right) \frac{d \ln \Sigma_2}{d \ln r} - \frac{d \ln \Omega_K}{d \ln r}\right], \quad (22)$$

with $A = 3(1 - \beta) + \beta/(\gamma - 1)$, $\beta = p_{\text{gas},2}/p_2$, and $\gamma = 5/3$ (Kato et al. 2008, Chapter 7.2).

3. NUMERICAL RESULTS

We propose the accretion timescale of Disk 1 to explain the CL timescale, expressed as $t_{\text{acc},1} = -r/v_1$. We assume that the UV/optical photons are emitted at $r = 50 r_s$, where $r_s = 2GM/c^2$ is the Schwarzschild radius (e.g., Feng et al. 2021; Wu & Gu 2023). We can numerically solve Equations (1), (5) ~ (9) and (14) ~ (18) for $t_{\text{acc},1}$ by employing the input parameters shown in Table 1.

The comparison of the timescales between SSD and our model is shown in Figure 2. For a typical AGN ($M \sim 10^7 - 10^8 M_\odot$, $\dot{M} \sim 0.01 - 0.1 \dot{M}_{\text{Edd}}$) with a SSD, the accretion timescale is longer than 10^3 yr, which is inconsistent with the observed CL timescale. In Figure 2, we employ $\dot{M}_2/\dot{M} = 0.1$ and $v_1/v_2 = 0.1$ to calculate $t_{\text{acc},1}$. The dotted and solid curves indicate that $t_{\text{acc},1}$ is two to three orders of magnitude shorter than SSD. For the condition that Disk 2 is dominated by the magnetic pressure ($\beta_m = 100$), $t_{\text{acc},1}$ is relatively longer than the case of negligible magnetic pressure in Disk 2 ($\beta_m = 0$). This result is contrary to Dexter & Begelman (2019), the magnetically elevated disk model, which shows that a magnetic pressure dominated disk will have a shorter accretion timescale. The reason for this lies in the difference of radiation mechanisms. The model proposed by Dexter & Begelman (2019) is an optically thick disk, therefore it is primarily cooled by blackbody radiation, and its cooling rate is approximated as $Q_{\text{bb}}^- \propto T^4/\tau_{\text{es}} \propto T^4/\Sigma$. Assuming that viscous dissipation is the only mechanism for angular momentum loss, the angular momentum equation is expressed as $\dot{M}(r^2\Omega_K - j) = 2\pi r^2\alpha\Pi$, where $\Pi = \Pi_{\text{gas}} + \Pi_{\text{mag}} + \Pi_{\text{rad}} = \text{constant}$. Therefore an increasing Π_{mag} will decrease Π_{gas} and Π_{rad} , resulting to a lower temperature. Our Disk 2 is primarily cooled by the bremsstrahlung radiation, and employing $\Sigma \propto \tau_{\text{es}} \propto \rho H$, $H_2 \propto (1 + \beta_m)^{1/2} T_2^{1/2}$ (from Equations (14) and (15), in our model $H_2 \gg H_1$), the cooling rate is approximated as $Q_{\text{brem},2}^- \propto \rho_2^2 H_2 T_2^{1/2} \propto \Sigma_2^2/(1 + \beta_m)^{1/2}$. Here we assume that Q_{bb}^- and Q_{brem}^- are constant and are not affected by β_m . Therefore, with the increasing of magnetic pressure, for a disk cooled by $Q_{\text{bb}}^- \propto T^4/\Sigma$, an increase in β_m will decrease T , resulting to a decrease of Σ , and considering that $\Sigma \propto v_r^{-1} \propto t_{\text{acc}}$, t_{acc} will be shorter. However, for a disk cooled by $Q_{\text{brem}}^- \propto \Sigma^2/(1 + \beta_m)^{1/2}$, as β_m increases, Σ also increases, which leads to a longer t_{acc} . Therefore, a magnetic pressure dominated Disk 2 will have a longer accretion timescale. As a result, under the condition of constant v_1/v_2 , the accretion timescale of Disk 1 also increases.

Figure 3 is the parameter space of v_1/v_2 and \dot{M}_2/\dot{M} for given ranges of $t_{\text{acc},1}$. We adapt $\dot{M} = 0.01 \dot{M}_{\text{Edd}}$, $M = 10^8 M_\odot$ as the typical input parameters for this figure. The regions corresponding to different accretion timescales are represented by different colors. Figure 3(a) is for the gas pressure dominated condition ($\beta_m = 0$) while (b) is for the magnetic pressure dominated condition ($\beta_m = 100$). The observed CL timescales can be easily explained by our model if Disk 2 is responsible for transporting the angular momentum of Disk 1, especially if Disk 2 is not magnetic pressure dominated.

Figure 4 shows the electron scattering optical depth and average temperature for Disk 2 with different β_m . Compared to the gas pressure dominated condition, the magnetic pressure dominated condition corresponds to greater $\tau_{\text{es},2}$ and lower \bar{T}_2 . Ballantyne et al. (2024) systematically analyzed the X-ray spectra of 14 Type 1 AGNs and determined the temperature and electron scattering optical depth of the warm coronae in these sources, which are $T \sim 10^7$ K and $\tau_{\text{es}} > 1$, respectively. Hence, our Disk 2 may account for the warm corona if Disk 2 is dominated by magnetic pressure.

4. CONCLUSIONS AND DISCUSSION

We have investigated a sandwich model to explain the timescales for CL-AGNs, including an optically thick disk (Disk 1) and two optically thin disks (Disk 2). In our model, Disk 1 is on the equatorial plane, with two optically thin disks above it on both sides. The interaction between Disk 1 and Disk 2 is generated by magnetic coupling, which causes Disk 1 losing angular momentum more quickly and decreases its accretion timescale. Our results indicate that, the accretion timescale for Disk 1 can be reduced by two to three orders of magnitude compared to SSD, which is responsible for the rapid variability of CL-AGNs. In addition, we also discuss the impact of magnetic pressure in Disk 2. When the magnetic pressure is negligible, Disk 2 manifests itself a “hot corona” and has a shorter accretion timescale. And when the magnetic pressure is two orders of magnitude stronger than the gas pressure, Disk 2 resembles a “warm corona” and has a longer accretion timescale.

The self-consistency of our model is verified by the effective optical depth τ_* . We have confirmed that within the parameter range shown in Table 1, $\tau_{*,1} > 1$ and $\tau_{*,2} < 1$ can be ensured. For Disk 1, the cooling is dominated by

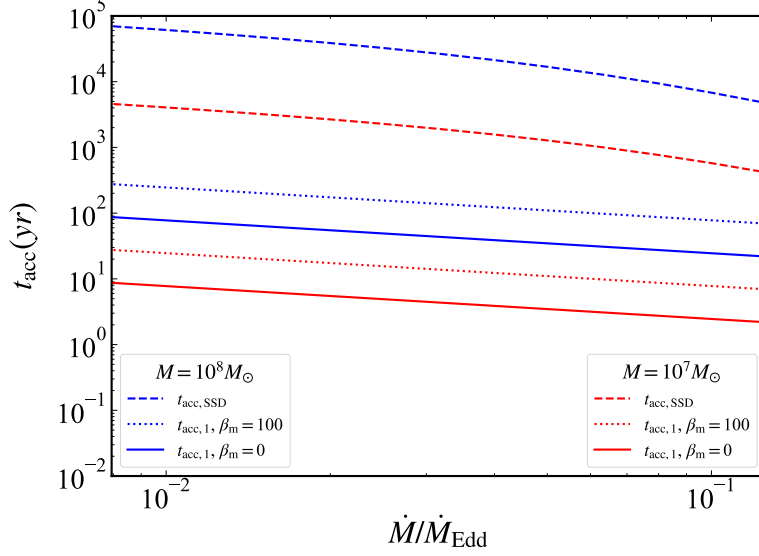


Figure 2. The accretion timescales for SSD and our Disk 1 at $r = 50 r_s$. In the timescale calculation, we fix $\dot{M}_2/\dot{M} = 0.1$ and $v_1/v_2 = 0.1$. Compare to SSD, our Disk 1 has much shorter accretion timescales.

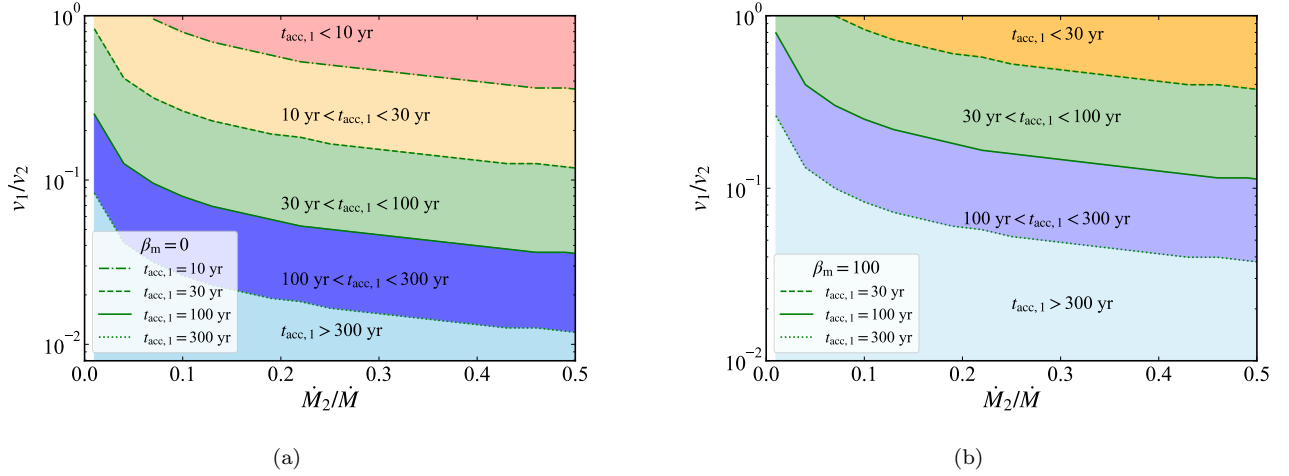


Figure 3. The ranges of $t_{\text{acc},1}$ as a function of v_1/v_2 and \dot{M}_2/\dot{M} . The other input parameters: $M = 10^8 M_\odot$, $\dot{M} = 0.01 \dot{M}_{\text{Edd}}$. The left and right panels correspond to gas pressure dominated and magnetic pressure dominated conditions, respectively.

the blackbody radiation for $\tau_* > 1$ (e.g., [Wandel & Liang 1991](#); [Narayan & Yi 1995](#)), while for Disk 2, $\tau_* < 1$ and the bremsstrahlung radiation is the main cooling mechanism. In addition, for $t_{\text{acc},1} < 100$ yr, the stress I owing to the strong magnetic coupling is three to four orders of magnitude stronger than the viscous stress generated by Disk 1 ($I \gg \alpha \Pi_1$). We speculate that the magnetic coupling in most AGNs is not strong, and only in CL-AGNs, this mechanism is significant, which may explain the small proportion of CL-AGNs.

In our model, the heating mechanism of Disk 2 is the viscous heating, which can be self-consistently calculated. Additionally, our model explains both the short timescale and the warm corona observed in CL-AGNs. The warm corona is associated with soft X-ray excess, which is usually observed in Type 1 AGNs (e.g., [Sobolewska & Done 2007](#); [Noda & Done 2018](#); [Ghosh et al. 2022](#); [Ballantyne et al. 2024](#)), and during the transition from Type 2 to Type 1 the soft X-ray excess appears (e.g., [Mathur et al. 2018](#); [Jana et al. 2021](#); [Kollatschny et al. 2023](#)). According to our model, we speculate that Disk 2 resembles the warm corona because of the increase of magnetic field and is responsible for

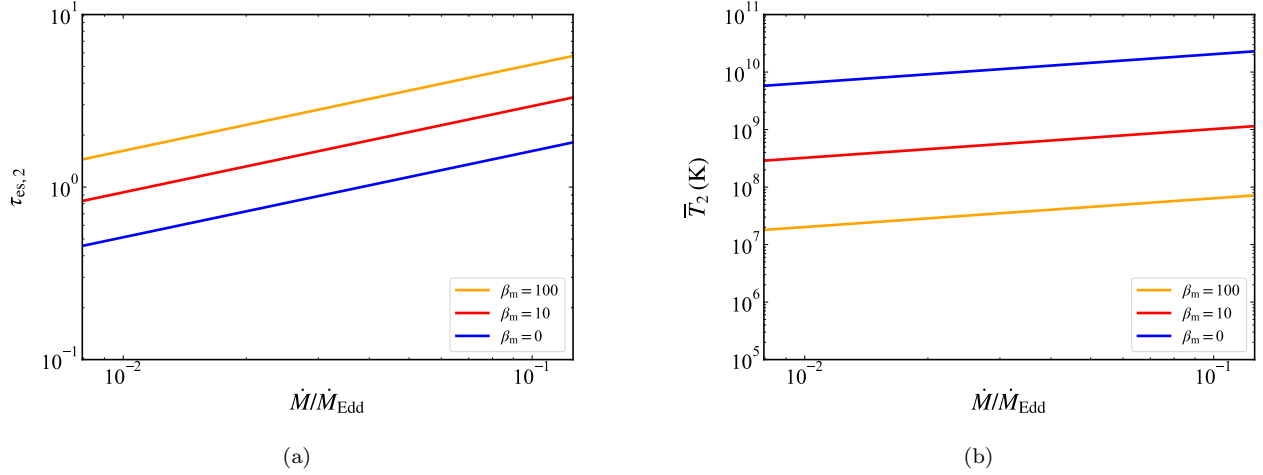


Figure 4. The electron scattering optical depth and average temperature of Disk 2 with different β_m . The other input parameters: $M = 10^8 M_\odot$, $\dot{M}_2/\dot{M} = 0.1$, and $v_1/v_2 = 0.1$.

the soft X-ray excess.

We thank the anonymous referee for constructive suggestions that improved the paper. This work was supported by the National Natural Science Foundation of China under grants 12033006, 12433007, 11925301, 12221003, 12233007, and 12322303.

REFERENCES

- Ballantyne, D. R., Sudhakar, V., Fairfax, D., et al. 2024, MNRAS, 530, 1603. doi:10.1093/mnras/stae944
- Cai, Z.-Y., Wang, J.-X., & Sun, M. 2020, ApJ, 892, 63. doi:10.3847/1538-4357/ab7991
- Cai, Z.-Y., Wang, J.-X., Zhu, F.-F., et al. 2018, ApJ, 855, 117. doi:10.3847/1538-4357/aab091
- Cao, X. 2009, MNRAS, 394, 207. doi:10.1111/j.1365-2966.2008.14347.x
- Cao, X., You, B., & Wei, X. 2023, MNRAS, 526, 2331. doi:10.1093/mnras/stad2877
- Cohen, R. D., Rudy, R. J., Puetter, R. C., et al. 1986, ApJ, 311, 135. doi:10.1086/164758
- Denney, K. D., De Rosa, G., Croxall, K., et al. 2014, ApJ, 796, 134. doi:10.1088/0004-637X/796/2/134
- Dexter, J. & Begelman, M. C. 2019, MNRAS, 483, L17. doi:10.1093/mnras/sly213
- Done, C., Davis, S. W., Jin, C., et al. 2012, MNRAS, 420, 1848. doi:10.1111/j.1365-2966.2011.19779.x
- Elitzur, M. 2012, ApJL, 747, L33. doi:10.1088/2041-8205/747/2/L33
- Feng, J., Cao, X., Li, J.-wen., et al. 2021, ApJ, 916, 61. doi:10.3847/1538-4357/ac07a6
- Ghosh, R., Laha, S., Deshmukh, K., et al. 2022, ApJ, 937, 31. doi:10.3847/1538-4357/ac887e
- Goodrich, R. W. & Miller, J. S. 1989, ApJL, 346, L21. doi:10.1086/185569
- Gu, W.-M. & Lu, J.-F. 2000, ApJL, 540, L33. doi:10.1086/312864
- Haardt, F. & Maraschi, L. 1993, ApJ, 413, 507. doi:10.1086/173020
- Hōshi, R. 1977, Progress of Theoretical Physics, 58, 1191. doi:10.1143/PTP.58.1191
- Husemann, B., Urrutia, T., Tremblay, G. R., et al. 2016, A&A, 593, L9. doi:10.1051/0004-6361/201629245
- Hutsemékers, D., Agís González, B., Marin, F., et al. 2020, A&A, 644, L5. doi:10.1051/0004-6361/202039760
- Hutsemékers, D., Agís González, B., Marin, F., et al. 2019, A&A, 625, A54. doi:10.1051/0004-6361/201834633
- Ichikawa, K., Packham, C., Ramos Almeida, C., et al. 2015, ApJ, 803, 57. doi:10.1088/0004-637X/803/2/57
- Jana, A., Kumari, N., Nandi, P., et al. 2021, MNRAS, 507, 687. doi:10.1093/mnras/stab2155
- Jiang, N., Wang, T., Dou, L., et al. 2021, ApJS, 252, 32. doi:10.3847/1538-4365/abd1dc
- Jiang, Y.-F., Stone, J. M., & Davis, S. W. 2014, ApJ, 784, 169. doi:10.1088/0004-637X/784/2/169
- Jin, J.-J., Wu, X.-B., & Feng, X.-T. 2022, ApJ, 926, 184. doi:10.3847/1538-4357/ac410c

- Kato, S., Fukue, J., & Mineshige, S. 2008, *Black-Hole Accretion Disks — Towards a New Paradigm —*, 549 pages, including 12 Chapters, 9 Appendices, ISBN 978-4-87698-740-5, Kyoto University Press (Kyoto, Japan), 2008.
- Kim, D.-C., Yoon, I., & Evans, A. S. 2018, *ApJ*, 861, 51. doi:10.3847/1538-4357/aac77d
- Kollatschny, W., Grupe, D., Parker, M. L., et al. 2023, *A&A*, 670, A103. doi:10.1051/0004-6361/202244786
- Kubota, A. & Done, C. 2018, *MNRAS*, 480, 1247. doi:10.1093/mnras/sty1890
- LaMassa, S. M., Cales, S., Moran, E. C., et al. 2015, *ApJ*, 800, 144. doi:10.1088/0004-637X/800/2/144
- Laor, A. & Netzer, H. 1989, *MNRAS*, 238, 897. doi:10.1093/mnras/238.3.897
- Li, S.-S., Feng, H.-C., Liu, H. T., et al. 2022, *ApJ*, 936, 75. doi:10.3847/1538-4357/ac8745
- Liang, W. C., Shu, X. W., Wang, J. X., et al. 2022, *Journal of High Energy Astrophysics*, 33, 20. doi:10.1016/j.jheap.2022.01.002
- Liu, B. F., Mineshige, S., Meyer, F., et al. 2002, *ApJ*, 575, 117. doi:10.1086/341138
- Liu, B. F., Mineshige, S., & Ohsuga, K. 2003, *ApJ*, 587, 571. doi:10.1086/368282
- Liu, H., Wu, Q., & Lyu, B. 2022, *ApJ*, 930, 46. doi:10.3847/1538-4357/ac5fa5
- MacLeod, C. L., Ross, N. P., Lawrence, A., et al. 2016, *MNRAS*, 457, 389. doi:10.1093/mnras/stv2997
- Malzac, J., Beloborodov, A. M., & Poutanen, J. 2001, *MNRAS*, 326, 417. doi:10.1046/j.1365-8711.2001.04450.x
- Mathur, S., Denney, K. D., Gupta, A., et al. 2018, *ApJ*, 866, 123. doi:10.3847/1538-4357/aadd91
- McElroy, R. E., Husemann, B., Croom, S. M., et al. 2016, *A&A*, 593, L8. doi:10.1051/0004-6361/201629102
- Merloni, A., Dwelly, T., Salvato, M., et al. 2015, *MNRAS*, 452, 69. doi:10.1093/mnras/stv1095
- Narayan, R., Kato, S., & Honma, F. 1997, *ApJ*, 476, 49. doi:10.1086/303591
- Narayan, R. & Yi, I. 1994, *ApJL*, 428, L13. doi:10.1086/187381
- Narayan, R. & Yi, I. 1995, *ApJ*, 452, 710. doi:10.1086/176343
- Neustadt, J. M. M., Hinkle, J. T., Kochanek, C. S., et al. 2023, *MNRAS*, 521, 3810. doi:10.1093/mnras/stad725
- Noda, H. & Done, C. 2018, *MNRAS*, 480, 3898. doi:10.1093/mnras/sty2032
- Oknyansky, V. L., Winkler, H., Tsygankov, S. S., et al. 2019, *MNRAS*, 483, 558. doi:10.1093/mnras/sty3133
- Osterbrock, D. E. & Ferland, G. J. 2006, *Astrophysics of gaseous nebulae and active galactic nuclei*, 2nd. ed. by D.E. Osterbrock and G.J. Ferland. Sausalito, CA: University Science Books, 2006
- Pan, X., Li, S.-L., & Cao, X. 2021, *ApJ*, 910, 97. doi:10.3847/1538-4357/abe766
- Parker, M. L., Komossa, S., Kollatschny, W., et al. 2016, *MNRAS*, 461, 1927. doi:10.1093/mnras/stw1449
- Parker, M. L., Scharrel, N., Grupe, D., et al. 2019, *MNRAS*, 483, L88. doi:10.1093/mnras/sly224
- Poutanen, J. & Svensson, R. 1996, *ApJ*, 470, 249. doi:10.1086/177865
- Ricci, C., Kara, E., Loewenstein, M., et al. 2020, *ApJL*, 898, L1. doi:10.3847/2041-8213/ab91a1
- Rózańska, A., Malzac, J., Belmont, R., et al. 2015, *A&A*, 580, A77. doi:10.1051/0004-6361/201526288
- Schnittman, J. D. & Krolik, J. H. 2010, *ApJ*, 712, 908. doi:10.1088/0004-637X/712/2/908
- Seyfert, C. K. 1943, *ApJ*, 97, 28. doi:10.1086/144488
- Shakura, N. I. & Sunyaev, R. A. 1973, *A&A*, 24, 337
- Sheng, Z., Wang, T., Ferland, G., et al. 2021, *ApJL*, 920, L25. doi:10.3847/2041-8213/ac2251
- Sheng, Z., Wang, T., Jiang, N., et al. 2017, *ApJL*, 846, L7. doi:10.3847/2041-8213/aa85de
- Sniegowska, M., Czerny, B., Bon, E., et al. 2020, *A&A*, 641, A167. doi:10.1051/0004-6361/202038575
- Sobolewska, M. A. & Done, C. 2007, *MNRAS*, 374, 150. doi:10.1111/j.1365-2966.2006.11117.x
- Stern, D., McKernan, B., Graham, M. J., et al. 2018, *ApJ*, 864, 27. doi:10.3847/1538-4357/aac726
- Sun, M., Xue, Y., Brandt, W. N., et al. 2020, *ApJ*, 891, 178. doi:10.3847/1538-4357/ab789e
- Trakhtenbrot, B., Arcavi, I., MacLeod, C. L., et al. 2019, *ApJ*, 883, 94. doi:10.3847/1538-4357/ab39e4
- Urry, C. M. & Padovani, P. 1995, *PASP*, 107, 803. doi:10.1086/133630
- Wandel, A. & Liang, E. P. 1991, *ApJ*, 380, 84. doi:10.1086/170564
- Wang, J., Xu, D. W., Wang, Y., et al. 2019, *ApJ*, 887, 15. doi:10.3847/1538-4357/ab4d90
- Wang, J., Xu, D. W., & Wei, J. Y. 2020, *ApJ*, 901, 1. doi:10.3847/1538-4357/abaa48
- Wang, J.-M. & Bon, E. 2020, *A&A*, 643, L9. doi:10.1051/0004-6361/202039368
- Wang, Y., Jiang, N., Wang, T., et al. 2022, *ApJS*, 258, 21. doi:10.3847/1538-4365/ac33a6
- Wu, W.-B. & Gu, W.-M. 2023, *ApJ*, 958, 146. doi:10.3847/1538-4357/acf839

Wyrzykowski, L., Zieliński, M., Kostrzewa-Rutkowska, Z.,
et al. 2017, MNRAS, 465, L114.
doi:10.1093/mnrasl/slw213

Yang, Q., Shen, Y., Liu, X., et al. 2019, ApJ, 885, 110.
doi:10.3847/1538-4357/ab481a

Yang, Q., Wu, X.-B., Fan, X., et al. 2018, ApJ, 862, 109.
doi:10.3847/1538-4357/aaca3a

Zetzl, M., Kollatschny, W., Ochmann, M. W., et al. 2018,
A&A, 618, A83. doi:10.1051/0004-6361/201732506

Zhang, X.-G. 2022, MNRAS, 517, L71.
doi:10.1093/mnrasl/slac110